

A SEARCH FOR THE HIGGS BOSON PRODUCED IN ASSOCIATION WITH TOP QUARKS IN MULTILEPTON FINAL STATES AT ATLAS

Chris Lester

A DISSERTATION
in
Physics and Astronomy

Presented to the Faculties of The University of Pennsylvania
in Partial Fulfillment of the Requirements for the Degree of Doctor of Philosophy
2014

Joseph Kroll, Professor, Physics
Supervisor of Dissertation

A.T. Charlie Johnson, Professor, Physics
Graduate Group Chairperson

Dissertation Committee

Randall Kamien, Professor, Physics

I. Joseph Kroll, Professor, Physics

Elliot Lipeles, Assistant Professor, Physics

Burt Ovrut, Professor, Physics

Joseph Kroll, Professor, Physics

A SEARCH FOR THE HIGGS BOSON PRODUCED IN ASSOCIATION WITH TOP QUARKS IN MULTILEPTON FINAL STATES AT ATLAS

COPYRIGHT
2014
Chris Lester

All rights reserved.

Acknowledgements

30 Acknowledgements acknowledgements acknowledgements acknowledgements acknowledgements ac-
31 knowledgements acknowledgements acknowledgements acknowledgements acknowledgements acknowl-
32 edgements acknowledgements acknowledgements acknowledgements acknowledgements acknowledgements
33 acknowledgements acknowledgements acknowledgements acknowledgements acknowledgements acknowledgements
34 acknowledgements acknowledgements acknowledgements acknowledgements acknowledgements acknowledgements
35 acknowledgements acknowledgements.

36 Acknowledgements acknowledgements acknowledgements acknowledgements acknowledgements ac-
37 knowledgements acknowledgements acknowledgements acknowledgements acknowledgements acknowledgements
38 acknowledgements acknowledgements acknowledgements acknowledgements acknowledgements acknowledgements
39 acknowledgements acknowledgements acknowledgements acknowledgements acknowledgements acknowledgements
40 acknowledgements acknowledgements acknowledgements acknowledgements acknowledgements acknowledgements
41 acknowledgements acknowledgements.

42 Acknowledgements acknowledgements acknowledgements acknowledgements acknowledgements ac-
43 knowledgements acknowledgements acknowledgements acknowledgements acknowledgements acknowledgements
44 acknowledgements acknowledgements acknowledgements acknowledgements acknowledgements acknowledgements
45 acknowledgements acknowledgements acknowledgements acknowledgements acknowledgements acknowledgements
46 acknowledgements acknowledgements acknowledgements acknowledgements acknowledgements acknowledgements
47 acknowledgements acknowledgements.

ABSTRACT

A SEARCH FOR THE HIGGS BOSON PRODUCED IN ASSOCIATION WITH TOP
50 QUARKS IN MULTILEPTON FINAL STATES AT ATLAS

Chris Lester

Joseph Kroll

Abstract abstract abstract abstract abstract abstract abstract abstract abstract
54 abstract abstract abstract abstract abstract abstract abstract abstract abstract
55 abstract abstract abstract abstract abstract abstract abstract abstract abstract
56 abstract abstract abstract abstract abstract abstract abstract abstract abstract
57 abstract abstract abstract abstract abstract abstract abstract abstract abstract
58 abstract abstract abstract abstract abstract abstract abstract abstract abstract
59 abstract abstract abstract abstract abstract abstract abstract abstract abstract
60 abstract abstract abstract abstract abstract abstract abstract abstract abstract
61 abstract abstract abstract abstract abstract abstract abstract abstract abstract.

Contents

63	Acknowledgements	iii
64	Abstract	iv
65	Contents	v
66	Preface	viii
67	1 Introduction	1
68	2 Theoretical Background	2
69	2.1 The Standard Model	2
70	2.1.1 The Standard Model Structure	2
71	2.1.2 Electroweak Symmetry Breaking and the Higgs	3
72	2.1.3 The Standard Model Parameters	4
73	2.2 Collider Physics and the Higgs	4
74	2.2.1 Higgs Discovery at the LHC	7
75	2.2.2 $t\bar{t}H$ Production	8
76	2.3 Conclusion	10
77	3 The Large Hadron Collider and the ATLAS Experiment	11
78	3.1 The Large Hadron Collider	11
79	3.1.1 The Accelerator Complex	11
80	3.1.2 Beam Parameters and Collisions	12
81	4 Electrons	14

82	4.1	Electrons at Hadron Colliders	14
83	4.2	Reconstruction of Electron at ATLAS	14
84	4.3	Identification of Electrons at ATLAS	14
85	4.3.1	Pile-up	14
86	4.3.2	Trigger vs. Offline	14
87	4.3.3	2011 Menu	14
88	4.3.4	2012 Menu	14
89	4.3.5	Electron Likelihood	14
90	4.4	Measurement of Electron Efficiency at ATLAS	14
91	4.4.1	Techniques	14
92	4.4.2	Issues	14
93	5	Search for the TTH Decay in the Multilepton Channel	15
94	5.1	Signal Characteristics	15
95	5.2	Background Overview	16
96	5.3	Analysis Strategy	17
97	6	Dataset and Simulation	18
98	6.1	Data	18
99	6.1.1	The 2012 Dataset	18
100	6.2	Simulation	19
101	6.2.1	Signal Simulation	20
102	6.2.2	Background Simulation	20
103	6.3	Analysis Overview and Signal Characteristics	21
104	7	Object and Event Selection	22
105	7.1	2l Same-Charge Signal Region	22
106	7.2	3l Signal Region	23
107	7.3	4l Signal Region	24
108	7.4	Electron Selection	24
109	7.5	Muon Selection	25
110	7.6	Jet and b-Tagged Jet Selection	25
111	7.7	Tau Selection	26
112	7.8	Object Summary and Overlap	26

113	7.9 Optimization	26
114	8 Conclusions	28
115	8.1 Higgs Results in Review	28
116	8.2 Prospects for Future	28
117	Bibliography	29

Preface

119 This is the preface. Blah blah blah blah blah blah. Blah blah blah blah blah blah. Blah
120 blah blah blah blah blah blah. Blah blah blah blah blah blah. Blah blah blah blah blah blah
121 blah. Blah blah blah blah blah blah. Blah blah blah blah blah blah. Blah blah blah blah
122 blah blah blah. Blah blah blah blah blah blah. Blah blah blah blah blah blah. Blah blah
123 blah blah blah blah. Blah blah blah blah blah blah. Blah blah blah blah blah blah.
124 Blah blah blah blah blah. Blah blah blah blah blah.

125 Blah blah blah blah blah blah. Blah blah blah blah blah blah. Blah blah blah blah blah
126 blah. Blah blah blah blah blah blah. Blah blah blah blah blah blah. Blah blah blah
127 blah blah blah. Blah blah blah blah blah blah. Blah blah blah blah blah blah. Blah
128 blah blah blah blah blah. Blah blah blah blah blah blah. Blah blah blah blah blah
129 blah. Blah blah blah blah blah blah. Blah blah blah blah blah blah. Blah blah blah
130 blah blah.

¹³²

CHAPTER 1

¹³³

Introduction

¹³⁴ Here is a citation [?].

135

CHAPTER 2

136

Theoretical Background

137 The Standard Model of particle physics (SM) is an extraordinarily successful description of the funda-
138 mental constituents of matter and their interactions. Experiments over the past 50 years have verified
139 the extremely precise prediction of the SM. This success has culminated most recently in the discovery
140 of the Higgs Boson. This chapter provides a brief introduction to the structure of the SM and how
141 scientists are able to test it using hadron collider but focuses primarily on the physics of the Higgs
142 boson and its decays to top quarks. Particular attention is given to the importance of a measurement
143 of the rate at which Higgs Bosons are produced in association of top quarks in the context of testing
144 the predictions the SM.

145 **2.1 The Standard Model**

146 **2.1.1 The Standard Model Structure**

147 The Standard Model (SM) [1, 2, 3, 4] is an example of a quantum field theory that describes the
148 interactions of all of the known fundamental particles. Particles are understood to be excitations of
149 the more fundamental object of the theory, the field. The dynamics and interactions of the fields are
150 derived from the Standard Model Lagrangian, which is constructed to be symmetric under transfor-
151 mations of the group $SU(3) \times SU(2) \times U(1)$. $SU(3)$ is the group for the color, $SU(2)$ is the group for
152 weak iso spin, and $U(1)$ is the group for weak hyper-charge.

153 Gauging the symmetries demands the introduction of 8 massless gluons, or the boson (full integer
154 spin) carriers of the strong force [5] from the generators $SU(3)$ symmetry, and the 4 massless bosons,
155 carriers for the weak and electromagnetic forces from the 3 generators of the $SU(2)$ and 1 generator
156 of the $U(1)$ group. The weak and the electromagnetic forces are considered part of a larger single

157 unified electroweak group $SU(2) \times U(1)$ and the associated generators mix.

158 The gauge symmetry allows the theory to be re-normalizable [6], meaning that unwanted infinities
 159 can be absorbed into observables from theory in a way that allows the theory to be able to predict
 160 physics at multiple energy scales. Singlets of the $SU(3)$ group are fermions (half-integer spin particles)
 161 called leptons and do not interact with the strong, whereas doublets of the $SU(3)$ group are called
 162 quarks and do interact with the strong force. The SM is a chiral theory: the weak force violates parity,
 163 as it only couples to left-chiral particles or right-chiral antiparticles. This means that right-chiral and
 164 left-chiral fermions arise from different fields, which are different representations of the weak isospin
 165 group.

166 The discovery of particles and new interactions in various experiments is intertwined with the
 167 development of the theory that spans many decades and is not discussed in detail here.

168 So far, 3 separate generations of both quarks and leptons have been discovered, differing only by
 169 mass. The gluon and the 4 electroweak bosons have also been discovered (W^+ , W^- , Z^0 , and γ) ¹. The
 170 reason for this 3-fold replication is not known.

171 2.1.2 Electroweak Symmetry Breaking and the Higgs

172 Despite the simple structure of theory, the discovery of massive fundamental particles creates two sets
 173 of problems both related to $SU(2) \times U(1)$. First, the force-carrying bosons must enter the theory
 174 without mass or the symmetries will be explicitly broken in the Lagrangian. Second, adding fermion
 175 masses to theory in an ad-hoc way allows the right-chiral and left-chiral fermions to mix. Since they
 176 possess different quantum numbers, as different representations of the weak-isospin group, this too
 177 breaks gauge invariance.

178 To solve these problems, spontaneous electro-weak symmetry breaking (EWSB) is introduced via
 179 the Brout-Englert-Higgs mechanism [7, 8, 9]. A massive scalar field in an electro-weak doublet is
 180 added to the theory with 4 new degrees of freedom and a potential which includes a quartic self-
 181 interaction term. Each fermion field interacts with the scalar field via a different Yukawa coupling,
 182 which unites the left and right chiral fields of a single particle type. This field explicitly preserves all
 183 of the symmetries, but the minimum of the potential does not occur when the expectation of the field
 184 is zero. The field eventually falls to a state, where it acquires a vacuum-expectation value. However,
 185 a non-zero field must therefore point in a particular direction of weak-isospin space, breaking the
 186 symmetry.

¹The actual particles observed to be produced and propagate may be linear combinations of the underlying generators (for the bosons) or gauge representations (for the fermions).

187 The consequences of this spontaneous symmetry breaking are tremendous. First, the universe
 188 is filled with a field with a non-zero expectation value. The theory can be expanded around this
 189 new value and 3 of the degrees of freedom can be interpreted as the longitudinal polarizations of
 190 the W^+ , W^- , and Z^0 , while the 4th remains a scalar field, called the Higgs field with an associated
 191 particle called the Higgs particle or "Higgs" The weak bosons acquire a mass via their longitudinal
 192 polarizations and the Yukawa couplings of the scalar field to the fermions now behave like a mass
 193 term at the this new minimum.

194 **2.1.3 The Standard Model Parameters**

195 Although the SM structure is set by specifying the gauge groups, the EWSB mechanism, and ac-
 196 knowledging the 3-fold replication of the fermions, confronting the SM with experiment requires the
 197 measurement of 17² free parameters, which are unconstrained from the theory. These free parameters
 198 include the fermion masses (from the Yukawa coupling), the force coupling constants, the angles and
 199 phase of the mixing between quarks, and constants from the Higgs and electroweak sector³.

200 Experiments have provided a number of measurements of the parameters of the SM[10]. Prior
 201 to the discovery of the Higgs boson (discussed later) the Higgs mass, however, was the only fully
 202 unconstrained parameter, although its value could be inferred via its involvement in loop corrections
 203 on the top mass (M_t) and the W mass (M_W). The GFitter collaboration assembles all relevant
 204 electroweak observable measurements into a statistical model and then allows certain measurements to
 205 float within their uncertainty to allow for a fit among multiple correlated measurements measurements
 206 [11]. Figure 2.1 shows the fitted constraints on 4 key SM parameters (M_H , M_W , M_t , $\sin^2\theta_w$) with
 207 actual measurements overlaid. The addition to the fit of the measured Higgs mass from the ATLAS
 208 and CMS collaborations creates a small tension, as the other observables prefer the mass to be much
 209 lower (~ 80 GeV/ c^2). The tension in the combined electroweak fit (including the Higgs) is not
 210 statistically significant with a p -value of 0.07.

211 **2.2 Collider Physics and the Higgs**

212 To test the theory, physicists accelerate particles to extremely high energies and force them to interact
 213 through collisions. Typically, the particles accelerated are electrons or protons, since they are stable.

²There are additional parameters from neutrino mass terms and mixing but it is unclear how to include these into the Standard Model, since it does not predict right-chiral neutrinos

³ The electroweak sector includes parameters like mass of the W^\pm and Z^0 bosons, the weak mixing angle, $\sin^2\theta_w$, the fermi constant G_F , and Higgs Mass and vacuum expectation value. These parameters however are not wholly independent. As discussed above, it is only necessary theoretically to specify the two parameters relevant to the Higgs potential and the two coupling associated with the gauge groups

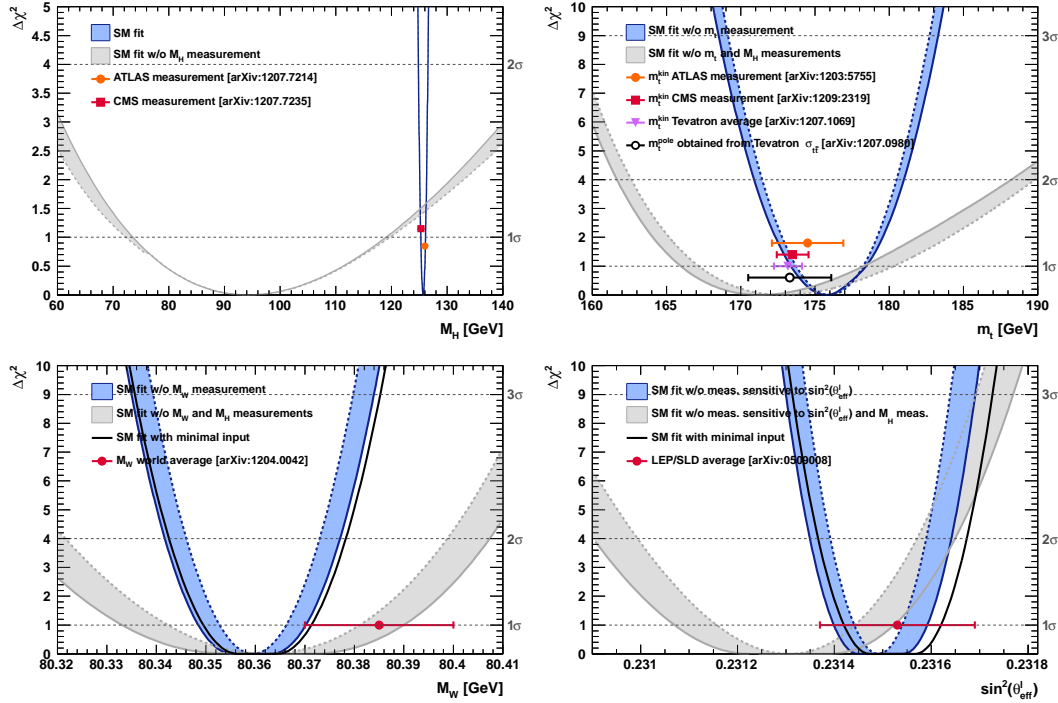


Figure 2.1: χ^2 as a function of the Higgs mass (top left), the top quark mass (top right), the W boson mass (bottom left) and the effective weak mixing angle (bottom right) for the combined SM fit from the GFitter group. The data points placed along $\chi^2 = 1$ represent direct measurements of the respective observable and their $\pm 1\sigma$ uncertainties. The grey (blue) bands show the results when excluding (including) the new M_H measurements from (in) the fits.

214 Electron-positron collider machines have a rich history of discovery and measurement in particle
 215 physics. The advantage of electron accelerators is that the colliding element is itself a fundamental
 216 particle. However, due to synchrotron radiation, curvature of the beam line becomes problematic for
 217 high energy beams. Hadron colliders, specifically, proton-proton and proton-anti-proton colliders can
 218 be accelerated in rings without large losses due to synchrotron radiation, but the actual colliding
 219 objects at high energies are the constituent quarks and gluons. This complicates analysis because the
 220 initial state of the system is not discernible on a per-collision basis and momentum of hard scatter
 221 system is unknown along the beam direction.

222 Collider physics rely on form-factor descriptions of the colliding hadrons that describe the fraction
 223 of momentum carried by the hadrons constituent ‘partons’. These are called parton-distribution
 224 functions, seen in Figure 2.2, and are factorized and integrated through the theoretical calculations
 225 of various collision processes [12].

226 At the Large Hadron Collider or LHC (discussed in detail in Chapter 3 a proton-proton colluder,

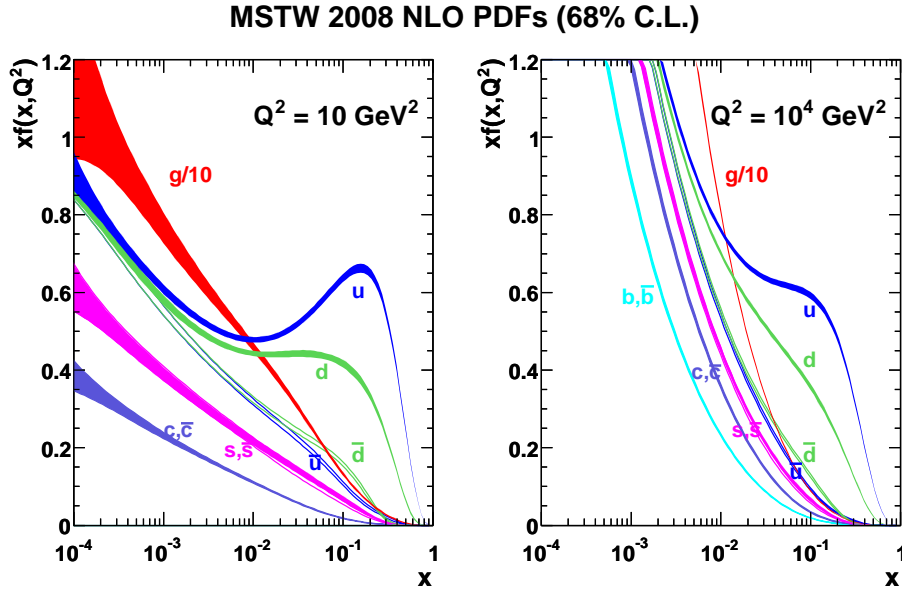


Figure 2.2: Proton Parton Distribution Functions (PDFs) form the MSTW Collaboration at $Q^2 = 10 \text{ GeV}^2$ and $Q^2 = 10^4 \text{ GeV}^2$

the types of initial states are quark-quark, quark-gluon, and gluon-gluon. Gluon collisions dominate overall, due to the large number of gluons inside the proton, though the relative importance of different initial states changes with the energy scale of the collision and the type of final state sought after.

A prime motivation for the construction of the Large Hadron Collider was the discovery or exclusion of the Higgs boson[13]. LEP and the Tevatron excluded large swaths of possible Higgs boson masses, especially below $114 \text{ GeV}/c^2$ and the unitarity of certain diagrams including the $WWWW$ vertex required the mass to be below about 1 TeV, a range that was achievable at the LHC with high luminosity running [10].

Despite the ubiquity of Higgs couplings, Higgs boson production at the LHC is a low rate process. Because it couples to fermions proportional to mass and because the colliding particles must be stable and therefore light, production of the Higgs must occur through virtual states.

The Higgs boson can be produced through collision at the LHC via 4 mechanisms: gluon-fusion (ggF), vector-boson fusion (VBF), Higgsstrahlung (VH), and production in association with top quarks ($t\bar{t}H$). The diagrams are shown in Figure 2.3 and the production cross-sections as a function of Higgs mass for the 8 TeV LHC proton-proton running are shown in Figure 2.4 [14]. The largest production cross-section is via the gluon fusion channel at 20 pb, which proceeds through a fermion loop that is dominated by the top quark, because of its large Yukawa coupling to the Higgs.

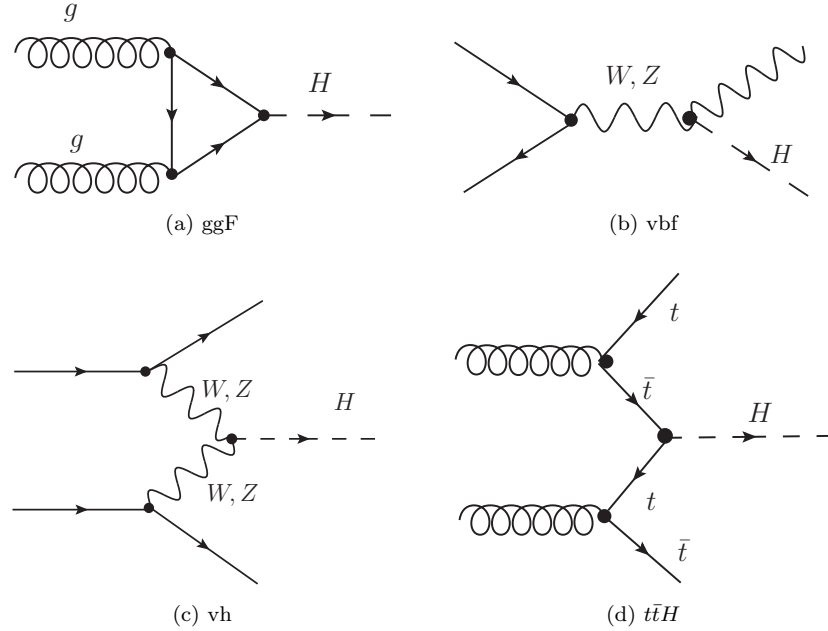


Figure 2.3: Dominant Higgs production modes at the LHC

Because the Higgs' couples to every massive particle, it has a rich set of decays also seen in Figure 2.4, especially for $m_H = 125$. Studies of Higgs properties at hadron colliders offers many tests of the Standard Model and ample room for searches for new physics. These tests specifically can verify the link between Yukawa coupling and the particles mass and further constrain details of EWSB by examining Higgs coupling to the weak bosons.

2.2.1 Higgs Discovery at the LHC

In 2012 both ATLAS and CMS announced the discovery of a new boson consistent with the Higgs by examining the results of Higgs searches in a number of decay channels ($H \rightarrow W^+W^-$, $H \rightarrow Z^0Z^0$, and $H \rightarrow \gamma\gamma$) in the 2011 dataset at $\sqrt{s} = 7$ TeV and part of the 2012 dataset at $\sqrt{s} = 8$ TeV. By 2013 and 2014, both experiments have updated and/or finalized their results for the full 2011 and 2012 datasets [15, 16]. I will focus on the ATLAS results in the following. The ATLAS measurements constrain both the Higgs mass[17] and spin[18], as well as provide constraints to the Higgs couplings to different particles.

Figure 2.5 show the results of the searches in all of the measurement channels as well as constraints on the SM Higgs coupling parameters in an example fit, where the couplings to the top-quark, bottom-

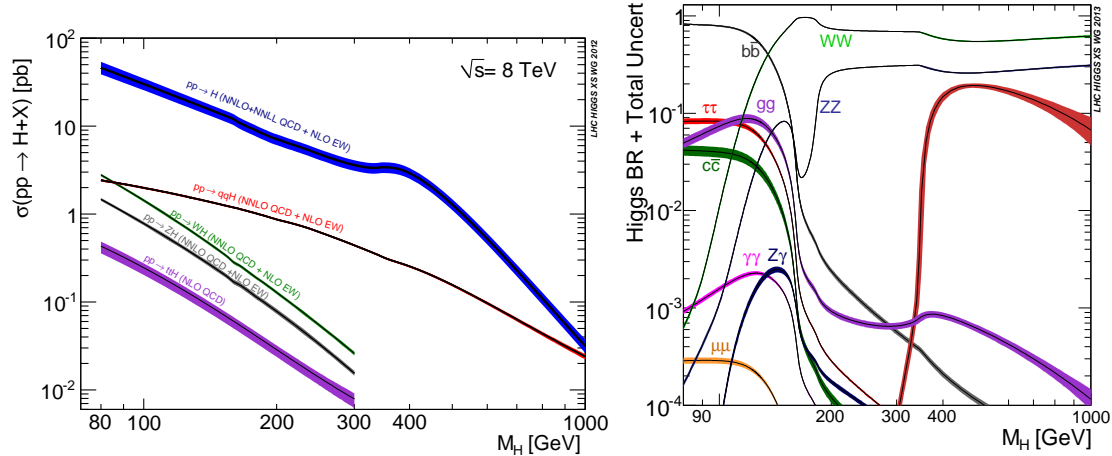


Figure 2.4: 8 TeV LHC Higgs production cross-sections (left) and decay branching fractions

quark, W,Z, and τ are allowed to fluctuate independently. These rely on measurements binned in different production and decay channels. They are dominated by higher statistics results in the gluon-fusion production modes, but measurements in the VH and VBF modes are close to SM sensitivity.

The combined results show basic agreement with the SM with much room for improvement with the addition of new production and decay modes and higher statistics. The coupling constraints are particularly strong for the W and Z, which are the most sensitive decay channels, and top quark due to the dominance of the top Yukawa in the ggF loop.

2.2.2 $t\bar{t}H$ Production

Notably absent thus far in the SM are searches for the Higgs in the $t\bar{t}H$ production channel, due to the lack of statistics. Searches are underway and initial results are close to SM sensitivity for ATLAS and CMS. More will be discussed about particular searches later. $t\bar{t}H$ production depends on the top Yukawa coupling at tree level. Comparison of the gluon-fusion and the $t\bar{t}H$ modes would allow for disentangling the effects of new particles in the gluon-fusion loop[19]. For instance, generic models would allow for the introduction of new colored particles into the loop. The simplest of these models would be the addition of a new generation of quarks. Fourth generation quarks, which obtain mass from a Higgs Yukawa coupling are already largely excluded due to their enormous effects on the Higgs production cross-section[20]. Other exotic scenarios allow for new colored particles in the gluon-fusion loop, which are not entirely constrained by present measurements[21, 22, 23]. These include, for instance, Supersymmetric models involving the stop quark.

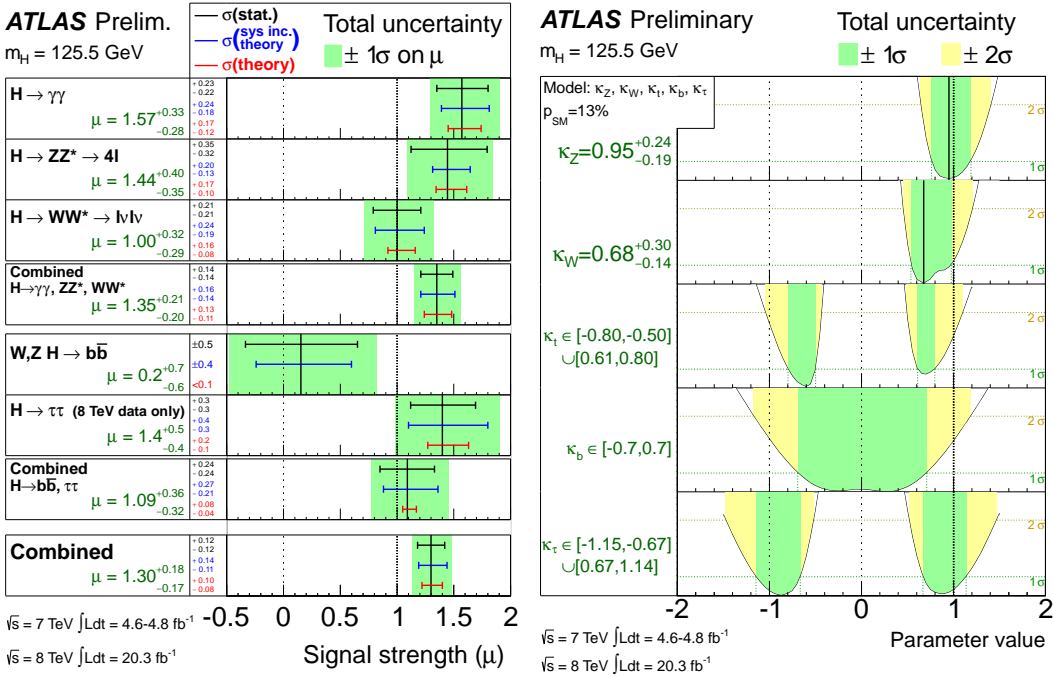


Figure 2.5: ATLAS Higgs combination results for all SM measurement channels as ratios of the measured to SM production cross-sections (left) and extracted Higgs coupling constraint scale-factors for a combined fit to the measurement channels, where the W, Z , top-quark, b -quark, and τ couplings are allowed to float. The p-value of this particular model is 0.13 and in agreement with SM expectations

Aside from the loop effects, measurement of the $t\bar{t}H$ production cross-section would provide a precise measurement of the top Yukawa coupling. When compared with the measured top quark mass, this tests the Higgs mass generation properties for up-type quarks. Despite similar uncertainties on the overall production cross-sections for $t\bar{t}H$ and the gluon-fusion modes, both of which depend on the top Yukawa, most of these uncertainties would cancel for $t\bar{t}H$ if normalized to the topologically similar $t\bar{t}Z$. Finally, the uniqueness of the experimental signature means that searches for $t\bar{t}$ signatures can be performed for a variety of Higgs decays ($\gamma\gamma, b\bar{b}, WW, ZZ$, and $\tau\bar{\tau}$) with roughly similar degrees of sensitivity (within a factor of 10)[19].

It is important to note the importance of the top Yukawa coupling to the overall structure of the SM, due to its enormous size compared to other couplings. The top Yukawa is for instance 350000x as large as the electron Yukawa coupling. Because of this the top Yukawa coupling, along with the Higgs mass, is one of the most important pieces of the renormalization group equations (RGE) responsible for the running of the parameter that determines the Higgs self-coupling λ . If this parameter runs negative, then the potential responsible for the entire mechanism of EWSB no longer has a minimum and becomes unbounded, resulting in instability in the universe [24]. Metastability occurs when the

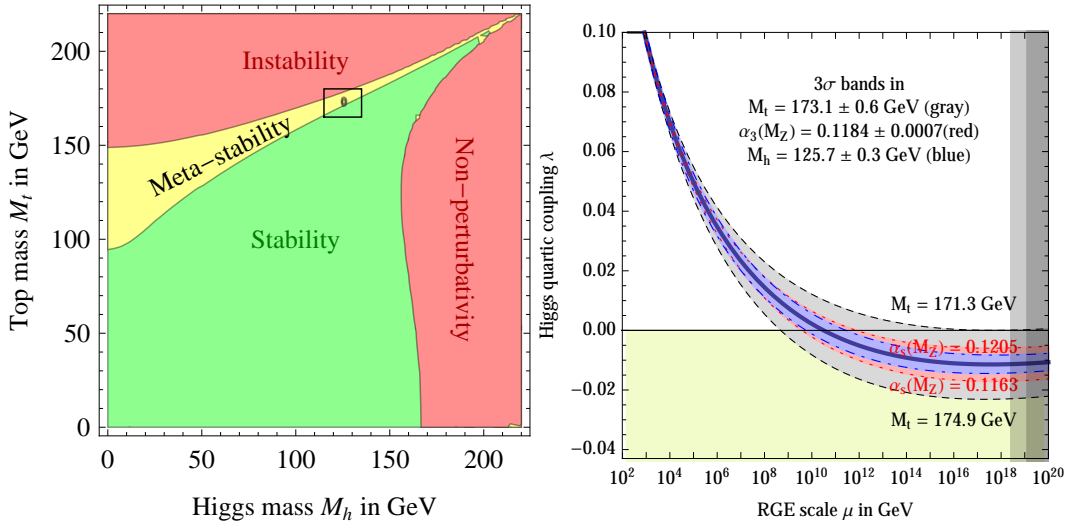


Figure 2.6: RGE for the running of the SM parameter, λ for the Higgs self-coupling term with present values and uncertainty bands for M_H and M_t (left). The two-dimensional plot colored (right) shows regions for which the SM is stable, unstable and metastable based on this RGE

shape of the potential allows for a false local minimum. Figure 2.6 shows the running of this parameter, the regions for which the universe is stable, unstable and metastable. Current measurements suggest that universe lies in a metastable island⁴.

2.3 Conclusion

The Standard Model, despite its success in providing a unified description of fundamental particles and interactions into single theory, has its flaws. These have been discussed in depth elsewhere, but include issues like the description of massive neutrinos, the failure to include gravity, and the unnaturalness of large quantum corrections to Higgs parameters. For these reasons, it seems the SM might be a lower energy approximation to a more fundamental theory. The discovery of the Higgs boson at the LHC provided a stunning verification of one of the fundamental aspects of the theory but at the same time offers new area to search for glimpses of something grander. The production of samples of Higgs bosons allows for a rich array of new tests of the Standard Model, which is now finally over-constrained by experiment. Searches for the $t\bar{t}H$ production, one category of which is the topic of this thesis, provide tree-level access to a central parameter of the theory, the top Yukawa coupling, as well as access a variety of Higgs decays, which will eventually provide a rigorous new test of the SM.

⁴The RGE assumed that there is no new physics at all energy scales

309

CHAPTER 3

310

The Large Hadron Collider and the ATLAS Experiment

311

312 3.1 The Large Hadron Collider

313 Production of a sufficient number of high energy collisions to adequately explore particle physics at
314 the electro-weak scale required the development of one of the most complex machines ever built, the
315 Large Hadron Collider or LHC.

316 The LHC is the world's highest energy particle accelerator and is located 100m underneath the
317 Franco-Swiss border at the European Organization for Nuclear Research (CERN) in a 26.7 km tunnel.

318 The technology involved in the development of the LHC and very briefly touched upon in this
319 chapter is an enormous achievement in its own right and is documented in detail here [25, 26, 27].

320 The LHC is a circular machine capable of accelerating beams of protons and colliding them at
321 center of mass energies up to $\sqrt{s} = 14\text{TeV}$ at 4 collision sites around the ring, where 4 experiments are
322 housed (ATLAS[28], CMS[?], LHCb[29], and ALICE[?]). Figure 3.1 is a diagram of the layout of the
323 LHC and its experiments[30]. The LHC also operates in modes with beams of heavy ions. The LHC
324 is composed of thousands of super-conducting Niobium-Titanium magnets, cooled to 2.7° C with
325 liquid Helium, which steer and focus the particle beams, and a superconducting resonant-frequency
326 (RF) cavity, which boosts the beam to higher energies.

327 3.1.1 The Accelerator Complex

328 The accelerator complex is a progressive series of machines with the LHC as the final stage. Protons are
329 obtained from hydrogen atoms and are accelerated to 50 MeV using the Linac2, before being injected
330 into the Proton-Synchrotron Booster (PSB). In the PSB the protons are accelerated to energies of 1.4

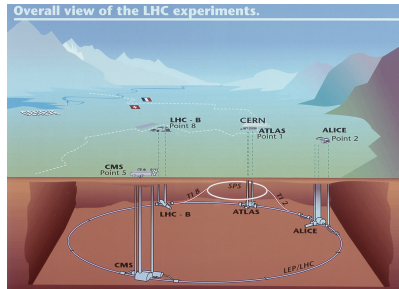


Figure 3.1: Diagram of the Large Hadron collider and location of the 4 main experiments (ATLAS, CMS, LHCb, and ALICE). Around the ring. The diagram also shows the location of the SPS, the final booster ring the accelerator complex that accelerates the protons to 450 GeV before injection into the LHC.

331 GeV for injection in to the Proton-Synchrotron (PS). The PS accelerates the protons to 25 GeV and
 332 dumps bunches into the Super Proton Synchrotron (SPS), where they are accelerated to 450 GeV
 333 and finally dumped into the LHC.

334 3.1.2 Beam Parameters and Collisions

335 For the physics studied at the ATLAS experiment, the two most important parameters of the collisions
 336 provided by the LHC are the center of mass energy and instantaneous luminosity. High center of mass
 337 energies are necessary for the production of new high mass particles, and because the constituents of
 338 the actual collisions are the partons of the proton, the CME of the collisions must in general be much
 339 higher than the mass of the particles needed to be produced. The

340 The instantaneous luminosity of the collisions, \mathcal{L} , is a measure of the collision rate. The integrated
 341 luminosity over time is a measure of the size of the dataset and when multiplied by the cross-section of a
 342 particular process gives the total number of expected events produced for that process. Instantaneous
 343 luminosity depends on the number of colliding bunches of protons, the intensity of those bunches, the
 344 revolution frequency, and the nomralized transverse spread of the beam in momentum and position
 345 phase space, called the emmitance, and the transverse beam size. The LHC has the option for colliding
 346 beams with 2808 bunches of protons, each with around 10^{11} protons, at a rate of one bunch collision
 347 every 25 ns, or 40 MHz. These correspond to a design luminosity of around $10^{34} \text{ cm}^2 \text{ s}^{-1}$ or 10 nb^{-1}

348 s⁻¹

349

CHAPTER 4

350

Electrons

351 **4.1 Electrons at Hadron Colliders**

352 **4.2 Reconstruction of Electron at ATLAS**

353 **4.3 Identification of Electrons at ATLAS**

354 **4.3.1 Pile-up**

355 **4.3.2 Trigger vs. Offline**

356 **4.3.3 2011 Menu**

357 **4.3.4 2012 Menu**

358 **4.3.5 Electron Likelihood**

359 **4.4 Measurement of Electron Efficiency at ATLAS**

360 **4.4.1 Techniques**

361 **4.4.2 Issues**

CHAPTER 5

Search for the TTH Decay in the Multilepton Channel

365 This chapter provides an overview of the set of analyses searching for the Standard Model (SM)
 366 production of the Higgs boson in association with top quarks in multi-lepton final states with multiple
 367 jets (including b-quark tagged jets). Searches in $t\bar{t}H$ final states with 2 same-charge, 3 and 4 light
 368 leptons (e, μ) are discussed in depth. These final states target specifically Higgs decays to vector
 369 bosons, $H \rightarrow W^\pm W^\pm$ and $H \rightarrow Z^\pm Z^\pm$ and form a complement to searches for $t\bar{t}H$ production in
 370 final states targeting the $H \rightarrow b\bar{b}$ [?], $H \rightarrow \gamma\gamma$ [?], and $H \rightarrow \tau\tau$ decay modes.

371 Based on SM production cross-sections, observation lies just outside the sensitivity of the Run I
 372 dataset, even when combining all searches. The analyses provide an opportunity to constrain for the
 373 first time the $t\bar{t}H$ production mode with limits reasonably close to the actual production rate. As
 374 such the analysis is optimized to overall sensitivity to the $t\bar{t}H$ production rather than individual decay
 375 modes, which would be more useful for constraining Higgs couplings.

376 Detailed description of the event and selection section are provided in Chapter 7, background
 377 modelling in Chapter ??, the effect of systematic errors and the statistical analysis in Chapter ?? and
 378 final results in Chapter ??.

379 **5.1 Signal Characteristics**

380 $t\bar{t}H$ can be observed in a number of different final states related to the Higgs boson and the top
 381 quark decay modes.

382 Three Higgs boson decays are relevant for this analysis: W^+W^- , $\tau^+\tau^-$ and ZZ . The top and
 383 anti-top quarks decay in $W^\pm b$. Each W^\pm boson decays either leptonically ($l=e^\pm, \mu^\pm, \tau^\pm$) with missing

384 energy or hadronically. Table 5.1 provides the fractional contribution of the main Higgs decay modes
385 at the generator level to $t\bar{t}H$ search channels. These numbers will be modified by lepton acceptances.

Table 5.1: Contributions of the main Higgs decay modes to the 3 multilepton $t\bar{t}H$ signatures at generation level.

Signature	$H \rightarrow WW$	$H \rightarrow \tau\tau$	$H \rightarrow ZZ$
Same-sign	100%	–	–
3 leptons	71%	20%	9%
4 leptons	53%	30%	17%

386 All modes are generally dominated by the WW signature, though the 3l and 4l channels possess
387 some contribution from the $\tau\tau$ and ZZ decays.

388 The signal is expected to be characterized by the presence of 2 b-quark jets from the top quark
389 decays, leptons from vector boson and tau decays, a high jet multiplicity, and missing energy. In
390 general, the number of leptons is anti-correlated with the number of jets, since a vector boson can
391 either decay leptonically or hadronically. For $H \rightarrow W^+W^-$, the light quark multiplicity, N_q , and the
392 number of leptons, N_l , follow this relation: $2N_l + N_q + N_b = 10$.

- 393 • In the same-sign channel, the $t\bar{t}H$ final state contains 6 quarks. These events are then characterised by a large jet multiplicity.
- 395 • In the 3 lepton channel, the $t\bar{t}H$ final state contains 4 quarks from the hard scatter.
- 396 • In the 4 lepton channel, the $t\bar{t}H$ final state contains a small number of light quarks, 0 ($H \rightarrow$
397 W^+W^- case), 2 or 4 ($H \rightarrow ZZ$ case).

398 5.2 Background Overview

399 Background processes can be sorted into two categories:

- 400 • Events with a non prompt or a fake lepton selected as prompt lepton. These processes cannot lead to a final state compatible with the signal signature without a misreconstructed object. This category includes events with a prompt lepton but with misreconstructed charge⁵ and events

5Charge mis-identification is almost exclusively a phenomenon of electrons at our energy scales. While it is possible for both electrons and muons to have an extremely straight track, whose direction of curvature is difficult to measure, this happens only at extremely high momentum. Electrons on the other hand may interact with the detector material, resulting in bremsstrahlung. The bremsstrahlung photon may subsequently convert resulting in 2 additional tracks near the original electron. This process, called a trident process, may cause a mismatching of the electron cluster with the original electron track and thus a charge-mis identification and happens also at low energies

403 with jets that "fake" leptons. These processes are rejected with tight object isolation and
404 identification criteria, requiring a large jet multiplicity, and veto-ing events consistent with a
405 leptonically decaying Z boson.

406 The main backgrounds of this sort are: $t\bar{t}$ and $Z+jets$. Data-driven techniques are used to
407 control some of these processes. Their importance varies depending on the channel.

- 408 • Events which can lead to the same final state as the signal (irreducible backgrounds). The
409 main background of this category are: $t\bar{t}V$, $W^\pm Z$, and ZZ . They are modeled using the
410 Monte Carlo simulations. In general, these backgrounds are combatted with jet and b-tagged
411 jet requirements. Although the jet multiplicity of $t\bar{t}V$ is high, the multiplicity of $t\bar{t}H$ events is
412 still higher.

413 **5.3 Analysis Strategy**

414 The analysis search is conducted in 3 channels, based on counting of fully identified leptons: 2 SS
415 leptons, 3 leptons, and 4 leptons. The lepton counting occurs before additional object cuts are made in
416 each individual channel to ensure orthogonality. The division into lepton channels rather than channels
417 targeting specific decay modes allows channels with different sensitivities to be considered separately. We
418 further divide the 2l SS into sub channels based on the number of jets and flavor of the leptons and
419 the 4l channel into subchannels enriched and depleted in OS leptons arising from Z decays.

420 The channels are fed into a posson model

421

CHAPTER 6

422

Dataset and Simulation

423 6.1 Data

424 6.1.1 The 2012 Dataset

425 The LHC successfully produced datasets for physics studies in 2010, 2011 and 2012. The 2012 proton-
426 proton dataset was delivered with collisions with a CME of 8 TeV with bunch collisions every 50 ns and
427 reached a total integrated luminosity of around 20 fb^{-1} [31]. Figure 6.1 shows the accumulation of this
428 dataset over time. Despite doubling the bunch spacing (thereby halving the bunch collision frequency),
429 the lumonisty neared the design lumonisty due to unexpected improvements in the transverse beam
430 profile[32]. This increased the amout of pile-up, or number of collisions per bunch crossing and in
431 general collision events were busier due to these multiple interactions. Figure 6.2 shows the average
432 number of interaction per bunch crossing for the 2011 and 2012 datasets. The 2012 dataset shows an
433 average of 20-25 interactions.

434 The $t\bar{t}H$ analysis uses the entire 2012 ATLAS dataset, collected from April to December. The size
435 of the dataset corresponds to 20.3 fb^{-1} , after passing data quality requirements, ensuring the proper
436 operation of the tracking, calorimeter and muon subsystems.

437 The datasets used in the analysis were collected with the primary electron (EF_E24VHL_MEDIUM1
438 — EF_E60_MEDIUM1) and muon triggers (EF_24I_TIGHT — EF_36_TIGHT). The electron
439 triggers require a electron with at least 25 GeV of calorimeter energy, passing the medium identification
440 requirement and loose tracking isolation. Above 60GeV, the isolation requirement is dropped and the
441 identification is loosened slightly. Similarly, the muon trigger requires a good inner detector track and
442 matching hits in the muon spectrometer, as well as loose tracking isolation, which also is dropped
443 about 36 GeVThe data sample must contain either a primary muon or primary electron trigger.

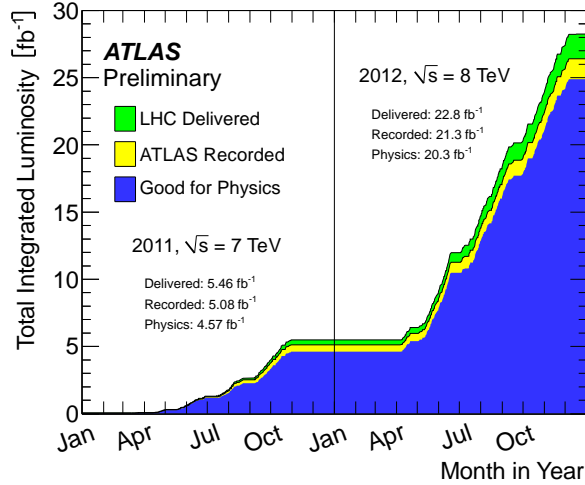


Figure 6.1: Plot showing the accumulation of the integrated luminosity delivered to the ATLAS experiment over 2011 and 2012. The rough size of the usable, physics ready dataset for 2012 is 20 fb^{-1} and is the dataset used for the following analysis.

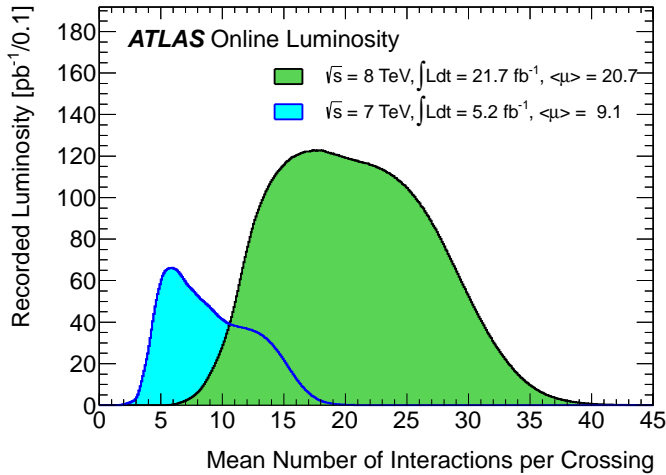


Figure 6.2: The average number of interactions per bunch-crossing for the 2012 and 2011 LHC proton-proton dataset. Most of these interactions are uninteresting but leave energetic signatures in particle detectors called pile-up which interfere with measurements

6.2 Simulation

Simulation samples based on are used to determine the overall event selection acceptance and efficiency and for investigations not directly involved in the final result. The simulated samples are created using parton distribution function (PDF) and model using Monte Carlo (MC) techniques the hard parton scatter, underlying event activity and parton showering and hadronization. The samples are then

Table 6.1: Monte Carlo samples used for signal description.

Process	Generator	Cross-section [fb]	\mathcal{L} [fb $^{-1}$]	Detector simulation
$t\bar{t}H \rightarrow \text{allhad} + H$	PowHel+Pythia8	59.09	2146.5	Full
$t\bar{t}H \rightarrow \text{ljets} + H$	PowHel+Pythia8	56.63	2238.9	Full
$t\bar{t}H \rightarrow ll + H$	PowHel+Pythia8	13.58	9332.0	Full

449 passed through a full ATLAS detector simulation[33] based on GEANT4 [34]. Small corrections are
 450 then applied to the overall efficiencies to re-scale object identification efficiencies, energy scales, and
 451 the pile-up, discussed in depth later.

452 6.2.1 Signal Simulation

453 The signal Monte Carlo samples are described in Table 6.1. These large samples are generated with
 454 inclusive Higgs boson decays, with branching fractions set to the LHC Higgs Cross Section Working
 455 Group (Yellow Report) recommendation for $m_H = 125$ GeV [?]. The matrix element calculation is
 456 performed at next-to-leading order (NLO); we use $t\bar{t}H$ Les Houches event format files provided by the
 457 authors of the PowHel software [?], decayed and showered with Pythia8[35]. The CT10[36] parton
 458 distribution function is used for matrix element generation. The inclusive cross section (129.3 fb at
 459 $m_H = 125$ GeV) is also obtained from the Yellow Report [?].

460 6.2.2 Background Simulation

461 The background simulations used for this analysis are listed in Table ???. In general, the Alpgen[37],
 462 MadGraph[38], and AcerMC[39] samples use the CTEQ6L1[40] parton distribution function, while
 463 the Powheg[41], Sherpa[42], are generated with the CT10 PDF. The exception is the MadGraph $t\bar{t}t\bar{t}$
 464 sample, which is generated with the MSTW2008 PDF[43]. The highest order calculations available
 465 are used for cross sections.

Table 6.2: Monte Carlo samples used for background description. Unless otherwise specified MadGraph samples use Pythia 6 for showering and Alpgen samples use Herwig+Jimmy.

Process	Generator	Detector simulation
$t\bar{t}W^\pm, t\bar{t}Z$	MadGraph	Full
tZ	MadGraph	AF2

Table 6.2: Monte Carlo samples used for background description. Unless otherwise specified MadGraph samples use Pythia 6 for showering and Alpgen samples use Herwig+Jimmy.

Process	Generator	Detector simulation
$t\bar{t}t\bar{t}$	MadGraph	Full
$t\bar{t}W^\pm W^\pm$	Madgraph+Pythia8	AF2
$t\bar{t}$	Powheg+Pythia6	Full/AF2
single top tchan	AcerMC+Pythia6	Full
single top schan $\rightarrow l$	Powheg+Pythia6	Full
single top $W^\pm t$	Powheg+Pythia6	Full
$W\gamma^*$	MadGraph	Full
$W\gamma+4p$	Alpgen	Full
W^+W^-	Sherpa	Full
$W^\pm Z$	Sherpa	Full
Same-sign WW	Madgraph+Pythia8	AF2
$ZZ \rightarrow$ Powheg+Pythia8,gg2ZZ+Herwig	Full	
$Z\gamma^*$	Sherpa	Full
$Z+jets$	Sherpa	Full
ggF_H(125)	Powheg+Pythia8	Full

466 6.3 Analysis Overview and Signal Characteristics

467 The signal

Table 6.3: Contributions of the main Higgs decay modes to the 5 multilepton $t\bar{t}H$ signatures at generation level.

Signature	$H \rightarrow WW$	$H \rightarrow \tau\tau$	$H \rightarrow ZZ$
Same-sign	100%	—	—
3 leptons	71%	20%	9%
4 leptons	53%	30%	17%

468

CHAPTER 7

469

Object and Event Selection

470 As stated in Chapter 5, the analysis is divided into 3 signal regions based on lepton counting: 2
471 same-charge leptons, 3 leptons and 4 leptons. The lepton counting occurs for fully identified leptons
472 with full overlap removal with transverse momentum over 10 GeV to ensure orthogonality. Lepton
473 selections are tightened afterward within each region.

474 The cuts for each signal region are provided in Table ?? and the object selections are detailed in
475 the following sections. The selections are based on optimizations of the region sensitivity performed
476 using MC (event for data driven backgrounds) and adhoc values for normalization systematic errors.
477 The optimziation is detailed in Section ?? . All signal regions are comprised of three basic requirements:
478 the presence of b-tagged jets, the presence of additional light jets, and a veto of same flavor opposite
479 sign leptons with an invariant mass within the Z window. Additional requirements on the invariant
480 mass of the leptons, the missing transverse energy in the event, and the total object energy (H_T)
481 proved to have negligible additional benefit at our level of statistics.

482 **7.1 2l Same-Charge Signal Region**

483 The 2 lepton same-charge signal region (2l SS) requires two leptons similar charge. The signal is
484 symmetric in charge but the background from $t\bar{t}$ di-lepton production is overwhelming, necessitating
485 the same-sign cut. Requiring only two leptons allows the extra 2 W bosons in the event to decay
486 hadronically, resulting in on average 4 additional light jets plus 2 additional b-quark jets from the top
487 decays.

488 A leading lepton with transverse momentum of at least 25 GeV/ c that matches to a trigger and a
489 subleading lepton of at least 20 GeV/ c , a b-tagged jet, and at least 4 jets in total are required.

490 In order to suppress non-prompt backgrounds, the lepton isolation criteria for tracking and

Table 7.1: Selections in the 2l SS, 3l and 4l Signal Regions

Signal Region	2l SS	3l	4l
Trigger Matched Lepton	Yes	Yes	Yes
N_l^{6}	=2	=3	=4
Lepton Charge Sum	+2 or -2	+1 or -1	0
Lepton Momentum (GeV/c^7)	$p_{T0} > 25$ $p_{T1} > 20$	$p_{T0} > 10$ $p_{T1,2} > 25, 20$	$p_{T0} > 25$ $p_{T1} > 20$ $p_{T2,3} > 10$
Jet Counting	$N_b \geq 1, N_{Jet} = 4$	$N_b \geq 1, N_{Jet} \geq 4$ or $N_b \geq 2, N_{Jet} = 3$	$N_b \geq 1, N_{Jet} \geq 2$
Mass Variables (GeV/c^2)	$ M_{ee} - M_Z < 10$	$ M_{SFOS} - M_Z < 10$	$M_{SFOS} > 10$ $150 < M_{4l} < 500$ $ M_{SFOS} - M_Z < 10$
Sub-channels	$2 (N_{Jet} = 4, N_{Jet} \geq 5)$ x 3 (ee, e μ , $\mu\mu$)	none	2 (No SFOS leps, SFOS leps)

491 calorimeter are tightened from less than 10% of the lepton momentum to 5%. To suppress charge mis-
 492 indentification, the electron is required to be extremely central ($|\eta| < 1.37$) to avoid the material-rich
 493 regions of the detector. Additionally, ee events with a lepton pair invariant mass within 10 GeV/c^2 of
 494 the Z pole are removed.

495 In order to maintain orthogonality with the τ analyses, events with fully identified taus are vetoed.
 496 For the statistical combination the channel is divided into 6 sub-channels: 2 jets counting bins
 497 ($N_{Jet} = 4, N_{Jet} \geq 5$) x 3 lepton flavor bins (ee, $\mu\mu$, e μ). The splitting allows

498 7.2 3l Signal Region

499 The 3 lepton channel requires 3 leptons, whose summed charge is either -1 or $+1$. The leptons are
 500 ordered in this way:

- 501 • lep0: the lepton that is opposite in charge to the other two leptons
- 502 • lep1: the lepton that is closer in ΔR to lep0
- 503 • lep2: the lepton that is farther in ΔR from lep1

504 Since events with a "fake" lepton arise from di-lepton processes, $t\bar{t}$ and Z+jets, where additional
 505 jets are mis-identified as the third lepton, lep0 is never the fake lepton. As a result, the transverse
 506 momentum requirement of lep0 is lower than the other two, $> 25 \text{ GeV}/c$. For the additional two
 507 leptons, one must match a trigger and have $p_T > 25 \text{ GeV}/c$ and the other must have $p_T > 10$
 508 GeV/c .

509 The 3l channel further requires at least one b-tagged jets and at least 4 jets in total, or two b-
 510 tagged jets and exactly 3 jets in total. Additionally, to suppress $W^\pm Z$ and Z+jet events, events with
 511 same-flavor opposite sign pairs within $10 \text{ GeV}/c^2$ of the Z pole are vetoed.

512 Additional cuts, including an M_{ll} cut, and splittings were investigated but low statistics proved
 513 to wash out any advantages.

514 **7.3 4l Signal Region**

515 In the four lepton signal region, selected events must have exactly four leptons with a total charge
 516 of zero. At least one leptons with must be matched to one of the applied single lepton trigger. The
 517 leading and sub-leading leptons are required to have a p_{T} of 25 and 15 GeV respectively. In order to
 518 suppress background contributions from low-mass resonances and Drell-Yan radiation, all opposite-
 519 sign-same-flavour (OS-SF) lepton pairs are required to have a dilepton invariant mass of at least 10
 520 GeV.

521 The four-lepton invariant mass is required to be between 100 and 500 GeV. This choice of mass
 522 window suppresses background from the on-shell $Z \rightarrow 4\ell$ peak and exploits the high-mass differences
 523 between the signal and the dominant $t\bar{t}Z$ background. Events containing an OS-SF lepton pair
 524 within 10 GeV of the Z boson mass are discarded. This Z-veto procedure greatly reduces background
 525 contributions from ZZ production as well as $t\bar{t}Z$ and while it also affects the signal by vetoing
 526 $H \rightarrow ZZ^*$, $Z \rightarrow \ell^+\ell^-$, these events constitute a small amount of the total expected signal. Finally,
 527 selected events are required to have at least two jets, at least one of which must be tagged as a b-quark
 528 initiated jet.

529 The contribution from $t\bar{t}Z$ comprises approximately 75% of the total background in the inclusive
 530 signal region. A signal region categorization which factorizes $t\bar{t}Z$ from the remaining backgrounds is
 531 thus beneficial. The signal region is accordingly divided into two categories based on the presence of
 532 OS-SF lepton pairs in the final state.

533 **7.4 Electron Selection**

534 The electrons are reconstructed by a standard algorithm of the experiment [?] and the electron
 535 cluster is required to be fiducial to the barrel or endcap calorimeters: $|\eta_{\text{cluster}}| < 2.47$. Electrons in
 536 the transition region, $1.37 < |\eta_{\text{cluster}}| < 1.52$, are vetoed. Electron reconstruction and identification
 537 is discussed in depth in Chapter 4. Electrons must pass the the VERYTIGHT likelihood identification
 538 criteria.

539 In order to reject jets (b-quark jets in particular) misidentified as electrons, electron candidate
 540 must also be well isolated from additional tracks and calorimeter energy around the electron cluster.
 541 Both the tracking and calorimeter energy within $\Delta R = 0.2$ of the electron cluster must be less
 542 than 5% of the electron transverse momentum: $ptcone20/P_t < 0.05$ and $Etcone20/E_T < 0.05$. All
 543 quality tracks with momentum greater than 400 MeV contribute to the isolation energy. Calorimeter
 544 isolation energy is calculated using topological clusters with corrections for energy leaked from the
 545 electron cluster [?]. Pile-up and underlying event corrections are applied using a median ambient
 546 energy density correction, developed in [?].

547 The electron track must also match the primary vertex. The longitudinal projection of the track
 548 along the beam line, $z0 \sin \theta$, must be less than 1 cm) and the transverse projection divided by the
 549 parameter error, $d0$ significance, must be less than 4. These cuts are used in particular to suppress
 550 backgrounds from conversions, heavy-flavor jets and electron charge-misidentifications.

551 The electron selection is provided in Table ??.

552 7.5 Muon Selection

553 Muons used in the analysis are formed by matching reconstructed inner detector tracks with either
 554 a complete track or a track-segment reconstructed in the muon spectrometer (MS). The muons must
 555 satisfy $|\eta| < 2.5$. The muon track are required to be a good quality combined fit of inner detector
 556 hits and muon spectrometer segments, unless the muon is not fiducial to the inner detector, $|\eta| > 2.4$.
 557 Muons with inner detector tracks are further required to pass standard inner detector track hit
 558 requirements [?].

559 As with electrons, muons are required to be isolated from additional tracking or calorimeter energy:
 560 $ptcone20/P_t < 0.1$, $Etcone20/E_T < 0.1$) A cell-based $Etcone20/P_T$ relative isolation variable is used.
 561 A pile-up energy subtraction based on the number of reconstructed vertices in the event is applied.
 562 The subtraction is derived from a Z boson control sample.

563 The muons must also originate from the primary vertex and have impact parameter requirements,
 564 $d0$ significance < 3 , and $z0 \sin \theta < 0.1$ cm, similar to the electrons.

565 The muon selection is provided in Table ??.

566 7.6 Jet and b-Tagged Jet Selection

567 Jets are reconstructed in the calorimeter using the anti- k_t [?] algorithm with a distance parameter of
 568 0.4 using locally calibrated topologically clusters as input (LC Jets).

569 Jets must pass loose quality requirement, ensuring the proper functioning of the calorimeter at the
570 time of data taking. Jets near a hot Tile cell in data periods B1/B2 are rejected. The local hadronic
571 calibration is used for the jet energy scale, and ambient energy corrections are applied to account for
572 energy due to pileup.

573 p_T and η cuts are tuned based on the sensitivity to $t\bar{t}H$ as explained in section ??.

574 For jets within $|\eta| < 2.4$ and $p_T < 50$ GeV, are required to be associated with the primary vertex,
575 the “jet vertex fraction” (or JVF), which is the fraction of track p_T associated with the jet that comes
576 from the primary vertex, must exceed 0.5 (or there must be no track associated to the jet).

577 B-jets are tagged using a Multi-Variate Analysis (MVA) method called MV1 and relying on infor-
578 mation of the impact parameter and the reconstruction of the displaced vertex of the hadron decay
579 inside the jet. The output of the tagger is required to be above 0.8119 which corresponds to a 70%
580 efficient Working Point (WP).

581 **7.7 Tau Selection**

582 The tau selection is important only in the 2l SS channel, due the tau veto to ensure orthogonality
583 with analyses searching for tau final states for a future combination.

584 **7.8 Object Summary and Overlap**

585 **7.9 Optimization**

Parameter	Values	Remarks
Electrons		
p_T	$> 10 \text{ GeV}$	
$ \eta $	< 2.47 veto crack	
ID	Very Tight Likelihood	< 1.37 for 2l SS channel
Isolation	$E_{\text{T}}\text{Cone}20/p_T, p_{\text{T}}\text{Cone}20/p_T < 0.05$	
Jet overlap removal	$\Delta R > 0.3$	
$ d_0^{\text{sig}} $	$< 4\sigma$	
$z_0 \sin\theta$	$< 1 \text{ cm}$	
Muons		
p_T	$> 10 \text{ GeV}$	
$ \eta $	< 2.5	
ID	Tight	
Jet overlap removal	$\Delta R > 0.04 + 10 \text{ GeV}/p_T$	
Isolation	$E_{\text{T}}\text{Cone}20/p_T, p_{\text{T}}\text{Cone}20/p_T < 0.1$	< 0.05 for 2 leptons
$ d_0^{\text{sig}} $	$< 3\sigma$	
z_0	$< 1 \text{ cm}$	
Taus		
p_T	$> 25 \text{ GeV}$	
ID	Medium BDT	
Isolation		
Jet overlap removal	$\Delta R > 0.3$	
e/μ vetoes	Medium electron veto	
Jets		
p_T	$> 25 \text{ GeV}$	
$ \eta $	< 2.5	
JVF	$\text{JVF} > 0.5$ or no associated track or $p_T > 50 \text{ GeV}$	
b-Tag	MV1 70% operating point	

Table 7.2: Object identification and selection used to define the 5 channels of the multilepton $t\bar{t}H$ analysis. Some channels use a sub-sample of objects as precised in the *Remarks* column.

586

CHAPTER 8

587

Conclusions

588 **8.1 Higgs Results in Review**

589 **8.2 Prospects for Future**

Bibliography

- 591 [1] S. L. Glashow, *Partial-symmetries of weak interactions*, Nucl. Phys. **22** (1961) no. 4, 579. [2.1.1](#)
- 592 [2] S. Weinberg, *A Model of Leptons*, Phys. Rev. Lett. **19** (1967) 1264. [2.1.1](#)
- 593 [3] A. Salam and J. C. Ward, *Gauge theory of elementary interactions*, Phys. Rev. **136** (1964)
594 763–768. [2.1.1](#)
- 595 [4] S. Weinberg, *Non-abelian gauge theories of the strong interactions*, Phys. Rev. Lett. **31** (1973)
596 494–497. [2.1.1](#)
- 597 [5] D. J. Gross and F. Wilczek, *Ultraviolet behavior of non-abelian gauge theories*, Phys. Rev. Lett.
598 **30** (1973) 1343–1346. [2.1.1](#)
- 599 [6] G. 't Hooft and M. Veltman, *Regularization and renormalization of gauge fields*, Nuclear
600 Physics B **44** (1972) 189 – 213. [2.1.1](#)
- 601 [7] P. W. Higgs, *Broken symmetries and the masses of gauge bosons*, Phys. Rev. Lett. **13** (1964)
602 508. [2.1.2](#)
- 603 [8] P. W. Higgs, *Spontaneous symmetry breakdown without massless bosons*, Phys. Rev. **145** (1966)
604 1156. [2.1.2](#)
- 605 [9] F. Englert and R. Brout, *Broken Symmetry and the Mass of Gauge Vector Mesons*,
606 Phys. Rev. Lett. **13** (1964) 321–322. [2.1.2](#)
- 607 [10] The ALEPH, CDF, DØ, DELPHI, L3, OPAL, SLD Collaborations, the LEP Electroweak
608 Working Group, the Tevatron Electroweak Working Group, and the SLD electroweak and
609 heavy flavour groups, *Precision Electroweak Measurements and Constraints on the Standard
610 Model*, CERN-PH-EP-2010-095 (2010) , arXiv:1012.2367 [hep-ex]. [2.1.3](#), [2.2](#)
- 611 [11] M. Baak, M. Goebel, J. Haller, A. Hoecker, D. Kennedy, R. Kogler, K. Mnig, M. Schott, and
612 J. Stelzer, *The electroweak fit of the standard model after the discovery of a new boson at the
613 LHC*, The European Physical Journal C **72** (2012) no. 11, .
614 <http://dx.doi.org/10.1140/epjc/s10052-012-2205-9>. [2.1.3](#)
- 615 [12] J. C. Collins, D. E. Soper, and G. Sterman, *Factorization for short distance hadron-hadron
616 scattering*, Nuclear Physics B **261** (1985) 104 – 142. [2.2](#)
- 617 [13] CERN, . CERN, Geneva, 1984. [2.2](#)

- 618 [14] LHC Higgs Cross Section Working Group, S. Dittmaier, C. Mariotti, G. Passarino, and
 619 R. Tanaka (Eds.), *Handbook of LHC Higgs Cross Sections: 2. Differential Distributions*,
 620 CERN-2012-002 (CERN, Geneva, 2012) , [arXiv:1201.3084 \[hep-ph\]](https://arxiv.org/abs/1201.3084). 2.2
- 621 [15] *Updated coupling measurements of the Higgs boson with the ATLAS detector using up to 25*
 622 fb^{-1} *of proton-proton collision data*, Tech. Rep. ATLAS-CONF-2014-009, CERN, Geneva, Mar,
 623 2014. 2.2.1
- 624 [16] CMS Collaboration Collaboration, *Precise determination of the mass of the Higgs boson and*
 625 *studies of the compatibility of its couplings with the standard model*, Tech. Rep.
 626 CMS-PAS-HIG-14-009, CERN, Geneva, 2014. 2.2.1
- 627 [17] ATLAS Collaboration Collaboration, G. Aad et al., *Measurement of the Higgs boson mass from*
 628 *the $H \rightarrow \gamma\gamma$ and $H \rightarrow ZZ^* \rightarrow 4\ell$ channels with the ATLAS detector using 25 fb^{-1} of pp*
 629 *collision data*, [arXiv:1406.3827 \[hep-ex\]](https://arxiv.org/abs/1406.3827). 2.2.1
- 630 [18] *Evidence for the spin-0 nature of the Higgs boson using {ATLAS} data*, Physics Letters B **726**
 631 (2013) no. 13, 120 – 144.
 632 <http://www.sciencedirect.com/science/article/pii/S0370269313006527>. 2.2.1
- 633 [19] S. Dawson, A. Gritsan, H. Logan, J. Qian, C. Tully, et al., *Working Group Report: Higgs*
 634 *Boson*, [arXiv:1310.8361 \[hep-ex\]](https://arxiv.org/abs/1310.8361). 2.2.2
- 635 [20] O. Eberhardt, G. Herbert, H. Lacker, A. Lenz, A. Menzel, et al., *Impact of a Higgs boson at a*
 636 *mass of 126 GeV on the standard model with three and four fermion generations*,
 637 Phys.Rev.Lett. **109** (2012) 241802, [arXiv:1209.1101 \[hep-ph\]](https://arxiv.org/abs/1209.1101). 2.2.2
- 638 [21] M. Carena, S. Gori, N. R. Shah, C. E. Wagner, and L.-T. Wang, *Light Stops, Light Staus and*
 639 *the 125 GeV Higgs*, JHEP **1308** (2013) 087, [arXiv:1303.4414](https://arxiv.org/abs/1303.4414). 2.2.2
- 640 [22] N. Arkani-Hamed, K. Blum, R. T. D’Agnolo, and J. Fan, *2:1 for Naturalness at the LHC?*,
 641 JHEP **1301** (2013) 149, [arXiv:1207.4482 \[hep-ph\]](https://arxiv.org/abs/1207.4482). 2.2.2
- 642 [23] D. Carmi, A. Falkowski, E. Kuflik, and T. Volansky, *Interpreting LHC Higgs Results from*
 643 *Natural New Physics Perspective*, JHEP **1207** (2012) 136, [arXiv:1202.3144 \[hep-ph\]](https://arxiv.org/abs/1202.3144). 2.2.2
- 644 [24] G. Degrassi, S. Di Vita, J. Elias-Miro, J. R. Espinosa, G. F. Giudice, et al., *Higgs mass and*
 645 *vacuum stability in the Standard Model at NNLO*, JHEP **1208** (2012) 098, [arXiv:1205.6497](https://arxiv.org/abs/1205.6497)
 646 [hep-ph]. 2.2.2
- 647 [25] L. Evans and P. Bryant, *LHC Machine*, JINST **3** (2008) no. 08, S08001. 3.1
- 648 [26] T. S. Pettersson and P. Lefevre, *The Large Hadron Collider: conceptual design.*, Tech. Rep.
 649 CERN-AC-95-05 LHC, CERN, Geneva, Oct, 1995. <https://cdsweb.cern.ch/record/291782>.
 650 3.1
- 651 [27] T. Linnecar et al., *Hardware and Initial Beam Commissioning of the LHC RF Systems.*
 652 [oai:cds.cern.ch:1176380](https://cds.cern.ch/record/1176380), Tech. Rep. LHC-PROJECT-Report-1172.
 653 CERN-LHC-PROJECT-Report-1172, CERN, Geneva, Oct, 2008.
 654 <https://cdsweb.cern.ch/record/1176380>. 3.1
- 655 [28] ATLAS Collaboration, *The ATLAS Experiment at the CERN Large Hadron Collider*, JINST **3**
 656 (2008) S08003. 3.1

-
- 657 [29] The LHCb Collaboration, *The LHCb Detector at the LHC*, *Journal of Instrumentation* **3** (2008)
658 no. 08, S08005. 3.1
- 659 [30] A. Team, *The four main LHC experiments*, Jun, 1999. 3.1
- 660 [31] ATLAS Collaboration, G. Aad et al., *Improved luminosity determination in pp collisions at \sqrt{s}*
661 $= 7 \text{ TeV using the ATLAS detector at the LHC}, *Eur.Phys.J.* **C73** (2013) 2518, arXiv:1302.4393
662 [hep-ex]. 6.1.1$
- 663 [32] CERN, . CERN, Geneva, 2012. 6.1.1
- 664 [33] ATLAS Collaboration Collaboration, G. Aad et al., *The ATLAS Simulation Infrastructure*,
665 *Eur.Phys.J.* **C70** (2010) 823–874, arXiv:1005.4568 [physics.ins-det]. 6.2
- 666 [34] GEANT4 Collaboration, S. Agostinelli et al., *GEANT4: A Simulation toolkit*,
667 *Nucl.Instrum.Meth.* **A506** (2003) 250–303. 6.2
- 668 [35] T. Sjostrand, S. Mrenna, and P. Z. Skands, *A Brief Introduction to PYTHIA 8.1*,
669 *Comput.Phys.Commun.* **178** (2008) 852–867, arXiv:0710.3820 [hep-ph]. 6.2.1
- 670 [36] H.-L. Lai, M. Guzzi, J. Huston, Z. Li, P. M. Nadolsky, et al., *New parton distributions for*
671 *collider physics*, *Phys.Rev.* **D82** (2010) 074024, arXiv:1007.2241 [hep-ph]. 6.2.1
- 672 [37] M. L. Mangano, M. Moretti, F. Piccinini, R. Pittau, and A. D. Polosa, *ALPGEN, a generator*
673 *for hard multiparton processes in hadronic collisions*, *JHEP* **0307** (2003) 001,
674 arXiv:hep-ph/0206293 [hep-ph]. 6.2.2
- 675 [38] F. Maltoni and T. Stelzer, *MadEvent: Automatic event generation with MadGraph*, *JHEP* **0302**
676 (2003) 027, arXiv:hep-ph/0208156 [hep-ph]. 6.2.2
- 677 [39] B. P. Kersevan and E. Richter-Was, *The Monte Carlo event generator AcerMC versions 2.0 to*
678 *3.8 with interfaces to PYTHIA 6.4, HERWIG 6.5 and ARIADNE 4.1*, *Comput.Phys.Commun.*
679 **184** (2013) 919–985, arXiv:hep-ph/0405247 [hep-ph]. 6.2.2
- 680 [40] P. M. Nadolsky, H.-L. Lai, Q.-H. Cao, J. Huston, J. Pumplin, et al., *Implications of CTEQ*
681 *global analysis for collider observables*, *Phys.Rev.* **D78** (2008) 013004, arXiv:0802.0007 [hep-ph].
682 6.2.2
- 683 [41] S. Frixione, P. Nason, and C. Oleari, *Matching NLO QCD computations with Parton Shower*
684 *simulations: the POWHEG method*, *JHEP* **0711** (2007) 070, arXiv:0709.2092 [hep-ph]. 6.2.2
- 685 [42] T. Gleisberg, S. Hoeche, F. Krauss, M. Schonherr, S. Schumann, et al., *Event generation with*
686 *SHERPA 1.1*, *JHEP* **0902** (2009) 007, arXiv:0811.4622 [hep-ph]. 6.2.2
- 687 [43] A. Martin, W. Stirling, R. Thorne, and G. Watt, *Parton distributions for the LHC*, *Eur.Phys.J.*
688 **C63** (2009) 189–285, arXiv:0901.0002 [hep-ph]. 6.2.2